Available online at www.sciencedirect.com
ScienceDirect
Journal of the European Ceramic Society 29 (2009) 3069–3077
www.elsevier.com/locate/jeurceramsoc

Effect of pyrolyzation temperature on wood-derived carbon and silicon carbide

K.E. Pappacena, S.P. Gentry [1], T.E. Wilkes [2], M.T. Johnson, S. Xie, A. Davis, K.T. Faber *

Department of Materials Science and Engineering, Northwestern University, 2220 N. Campus Drive, Evanston, IL 60208, USA

Received 4 March 2009; received in revised form 23 April 2009; accepted 30 April 2009
Available online 30 May 2009

Abstract

The structure of carbon and silicon carbide produced through the pyrolyzation of wood and the subsequent melt-infiltration with silicon was studied as a function of initial carbon pyrolyzation temperature. Scanning electron microscopy, transmission electron microscopy, mercury intrusion porosimetry, X-ray diffraction and Raman spectroscopy were used to characterize material derived from initial carbon pyrolyzation temperatures in the range of 300–2400 °C. It was determined that, although structural differences abound in carbon pyrolyzed at different temperatures, the resulting silicon carbide is independent of the initial temperature of carbon pyrolyzation.

Keywords: Porosity; Carbon; SiC; Spectroscopy; X-ray methods

1. Introduction

Biomorphic silicon carbide (bioSiC) utilizes a unique method of processing porous ceramics from wood. This technique involves the pyrolysis of natural wood precursors, followed by the infiltration of silicon to form silicon carbide (SiC), retaining the initial wood structure.[1–4] Utilizing the natural wood structure takes advantage of pre-existing porosity, thus eliminating high-energy pore-forming routes from the processing steps. There are many potential high-temperature applications for these porous ceramics, including heat exchangers, molten metal filters, catalyst supports, and heating elements.[4]

Hardwood microstructures include three types of pores: vessels, which are large diameter cells used for transportation of nutrients, and fibers and rays, which are smaller diameter cells used for strength and storage.[5] The vessels and fibers are elongated and run in the axial (longitudinal) direction of the tree. The rays are aligned perpendicularly to the vessels and fibers, in the transverse direction.[5] Depending on the wood species, the relative size and size distribution of the various pores can vary considerably. The mechanical and thermal properties of the resulting porous silicon carbide have been well characterized as a function of porosity and orientation.[3,4,6–8] The effects of the pyrolyzation temperature on the resulting silicon carbide, however, have not yet been determined.

Traditionally, to produce bioSiC, the carbon is pyrolyzed to 1000 °C, but previous research has shown that the majority of weight loss as a result of pyrolyzation occurs before the temperature has reached 500 °C.[7–9] However, X-ray diffraction of wood samples pyrolyzed from 400–2500 ° C showed a gradual narrowing of the (0 0 2) reflection (near $2\theta = 26°$) as the pyrolyzation temperature increased, indicating that although the weight loss is complete, some structural changes are occurring.[10] Although increased order is observed, wood-based carbon will not arrange into graphite, and thus is classified as non-graphitizable.[11] Strong cross-linked bonds are formed at low temperatures, such that even with high-temperature heat treatments (3000 °C), crystalline graphite never results.[11,12] Instead, turbostratic carbon is formed, characterized by misaligned graphene sheets with an average lattice spacing larger than that of graphite.

The goal of the current work is to investigate further the progression towards structural order in wood-derived carbon, and then determine how the pyrolyzation temperature affects the resulting silicon carbide material. While previous work has utilized X-ray diffraction to monitor structural changes of carbon pyrolyzed at different temperatures,[10] this work further explores

* Corresponding author.
E-mail address: k-faber@northwestern.edu (K.T. Faber).
[1] Present address: Department of Materials Science and Engineering, University of Michigan, Ann Arbor, Michigan 48109, USA.
[2] Present address: Ethicon, Inc., Somerville, NJ 08876, USA.

0955-2219/$ – see front matter © 2009 Elsevier Ltd. All rights reserved.
doi:10.1016/j.jeurceramsoc.2009.04.040

these structures through first studying the atomic level crystal structure with transmission electron microscopy, the bonding characteristics using Raman spectroscopy, and finally investigating the samples at a microscopic level by analyzing the pore size distribution using mercury porosimetry. In addition, the resultant SiC is similarly characterized, in order to determine the effect of the pyrolyzation temperature on the final ceramic product and optimize the processing conditions.

2. Experimental procedures

2.1. Materials processing

Carbon and biomorphic silicon carbide were processed from five hardwood precursors: beech (*Fagus sylvatica*), mahogany (*Swietenia macrophylla*), poplar (*Liriodendron tulipifera*), red oak (*Quercus rubra*) and sapele (*Entandrophragma cylindricum*).[13] Wood samples were cut and pyrolyzed at temperatures of 300, 500, 700, 1000 and 1200 °C in argon for one hour to produce carbon. These carbon scaffolds were subsequently melt-infiltrated at 1500 °C in vacuum for one hour with excess silicon powder to form silicon carbide. Unreacted silicon was removed using a continuously stirred mixture of HF/HNO_3.[7](For clarity, the initial carbon pyrolyzation temperature used to fabricate the carbon or silicon carbide sample will be added to the sample name, e.g. bioSiC 500 is bioSiC processed from carbon pyrolyzed at 500 °C). Beech wood was also pyrolyzed to 2400 °C in argon for 30 min commercially.

Additional samples of red oak- and mahogany-based carbon, pyrolyzed at each temperature, were reheated to 1500 °C in vacuum for one hour. This procedure, which will be referred to as mock infiltration, was done to simulate the conditions that the carbon is subjected to immediately prior to the start of melt-infiltration.

2.2. Characterization methods

Scanning electron microscopy (Hitachi S-3400N-II SEM, Hitachi High Technologies America Inc., Pleasanton, CA) and transmission electron microscopy (JEOL JEM-2100 FasTEM, JEOL USA, Inc., Peabody, MA) were used to investigate the microstructure of the carbon and biomorphic silicon carbide samples. Traditional transmission electron microscopy (TEM) sample preparation was done by thinning 3 mm diameter discs to a thickness of 100 μm using SiC grit paper on a grinding wheel, with further thinning to a 10 μm with a dimpler. The samples were then mounted on molybdenum grids followed by ion milling using a Gatan Model 691 Precision Ion Polishing System (Gatan, Inc., Pleasanton CA).

X-ray diffraction was performed using a Rigaku ATX-G diffractometer (Rigaku Americas, The Woodlands, Texas) operating at 50 kV and 240 mA, using Cu-K α radiation (1.54 Å). Powdered carbon samples (500 mg) were combined with a silicon standard (100 mg) to determine accurate peak locations. A $2\theta/\omega$ scan was performed at a scan rate of 3° min^{-1} with a step size of 0.05°, using 0.5 mm slits. Two known silicon peaks ($2\theta = 28.4^\circ$ and 47.3°) were used to establish a linear correction factor for the 2θ axis so that the location of the carbon signal could be compared from sample to sample. The intensity was normalized to the 28.4° silicon peak for each specimen to allow direct comparison of peak intensities from one sample to the next.

Raman spectroscopy (Acton TriVista CRS Confocal Raman System, Princeton Instruments, Trenton, NJ), with an operating current of 40 mA, and a laser of wavelength 514.5 nm, was used to characterize the carbon materials over a range of 1200–1800 cm^{-1}. For the carbon samples, the values were normalized to the height of the convoluted peak made up of the G (1580 cm^{-1}) and D2 (1620 cm^{-1}) peaks, as well as the minimum intensity value, in order to compare the curves from different samples directly. For the silicon carbide samples, a range of 700–1000 cm^{-1} was used and the spectra were normalized to the TO (796 cm^{-1}) peak and the minimum intensity value for direct comparison between samples.

An Autopore IV (Micromeritics, Norcross, GA) mercury porosimeter was used to determine the incremental intrusion of mercury with pressure, from which a volume percent for a particular pore diameter was calculated using:

$$\text{Volume}\% = \frac{I \times P}{T} \quad (1)$$

where I is the incremental intrusion, P is the porosity and T is the total intrusion. The pore diameters are determined from the Washburn equation, which relates pore diameter (d), pressure (p), wetting angle of Hg ($\theta = 130^\circ$), and surface tension between the Hg and the sample ($\gamma_{lv} = 485$ dynes/cm)[14] by:

$$p = \frac{2\gamma_{lv}}{d}\cos\theta \quad (2)$$

Eq. (2) assumes cylindrical pores, and the diameter measured represents the smallest opening for a particular pore space.

3. Results and discussion

3.1. Materials

Fig. 1(a)–(e) show examples of the microstructures of each wood precursor used in this study after pyrolyzation to 1000 °C, with their corresponding porosity values listed in each figure. It is obvious from these images that the microstructures vary greatly from wood to wood. Beech and poplar-based carbon, Fig. 1(a) and (b), respectively, have similar microstructures; the vessels are evenly distributed throughout the microstructure and are similar in size. However, they have vastly different porosities, ranging from 56–79%. Mahogany- and red oak-based carbon, Fig. 1(c) and (d), respectively, have similar porosity values, but have vastly different pore distributions. Mahogany has a bimodal pore size distribution, where large vessel-derived pores are dispersed throughout regions of smaller fiber-derived pores. In red oak, there is a trimodal distribution, with bands of larger and smaller vessel-derived pores surrounded by smaller fiber-derived pores. The resulting porous silicon carbide ceramic microstructures from the five wood precursors are shown in Fig. 2. It is apparent that these microstructures mimic those of

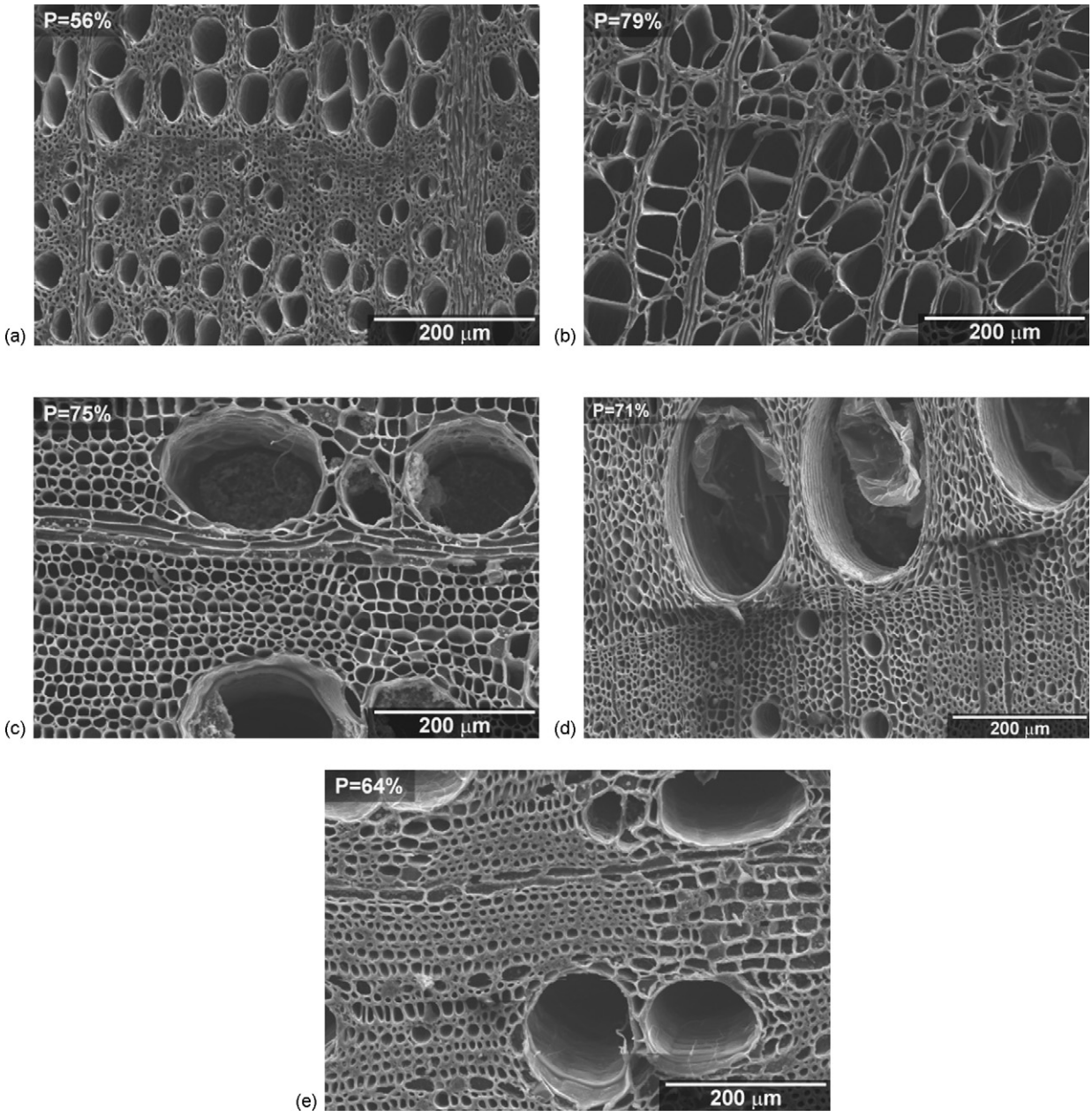

Fig. 1. Scanning electron micrographs of pyrolyzed wood from five precursors: (a) beech, (b) poplar, (c) mahogany, (d) red oak, and (e) sapele.

their carbon precursors in Fig. 1. In beech- and poplar-based materials, the struts break upon conversion to silicon carbide, causing the pores to coalesce.

The variation of the vessel size distribution from wood to wood is evident in Figs. 1 and 2, but is quantified with mercury porosimetry. Fig. 3(a) shows the pore size distribution of carbon pyrolyzed to 1000 °C from each of the five woods studied. The total porosity of each sample is listed to the right of its respective curve. Poplar has the most homogeneous distribution, with the majority of pore sizes ranging from 0.35–3.2 μm. Red oak-based carbon exhibits a trimodal distribution of pore sizes with both large and small vessels, as well as smaller fiber cells. Mahogany-based carbon, which has a bimodal distribution, contains some of the largest vessels seen, but the majority of the porosity derives from pores <0.7 μm. Beech- and sapele-based carbon also exhibit bimodal distributions, but the spread between the peaks representing the fiber-derived and vessel-derived pores is larger in sapele (0.05–61 μm) than beech (0.4–24 μm).

Fig. 3(b) shows the pore size distributions of bioSiC from the five different wood types derived from carbon pyrolyzed at 1000 °C. In all wood types, the smallest pores are eliminated due to the volume expansion of ∼58% associated with the silicon carbide formation reaction.[6] This shifts the pore size distribution in mahogany-, sapele- and red oak-based bioSiC such that there are no pores smaller than 1 μm. The majority of porosity in each of these woods is made up of large pores, greater than 60 μm in mahogany, 45 μm in sapele and 60 μm in red oak. Large pores, on average, also decrease in size due to carbide formation.

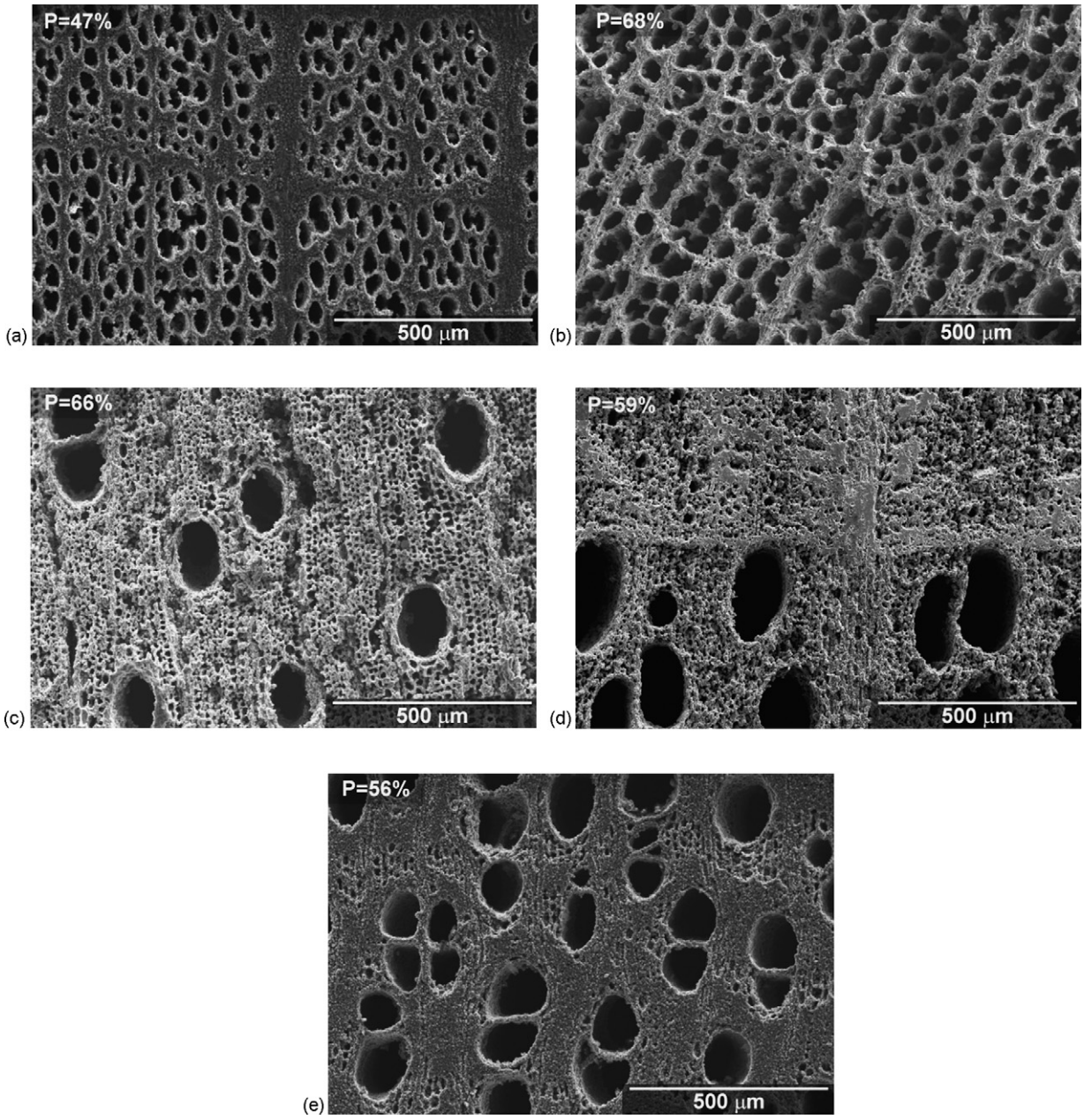

Fig. 2. Scanning electron microscope images of bioSiC derived from carbon pyrolyzed at 1000 °C from (a) beech, (b) poplar, (c) mahogany, (d) red oak, and (e) sapele woods (after reference [8]). Note the broken struts in the beech- and poplar-based bioSiC.

However, in the beech- and poplar-based bioSiC, the pore size distribution shifts towards larger sizes, which can be attributed to the breakage of struts during the expansion reaction, causing some pores to coalesce. This is further illustrated by comparison of carbon and bioSiC derived from both beech (Figs. 1(a) and 2(a)) and poplar (Figs. 1(b) and 2(b)) woods.

3.2. Pyrolyzation to carbon

The atomic structure of the carbon pyrolyzed at two temperatures was inspected using high resolution transmission electron microscopy (HRTEM). Fig. 4(a) and (b) are HRTEM images of carbon 300 and residual carbon present in the bioSiC 1000 sample, respectively. The carbon in both figures show similar amorphous structures, indicated by the lack of long-range order seen at the atomic level in these images. The carbon present in bioSiC 1000 (Fig. 4(b)) was first pyrolyzed to 1000 °C and subsequently reheated to 1500 °C. According to the HRTEM results, it does not exhibit any higher degree of crystallinity compared to the carbon pyrolyzed at only 300 °C. Thus, for these two heat treatments, there does not appear to be any significant difference in the resulting carbon materials at the atomic level.

X-ray diffraction results support the TEM observations. Plotted in Fig. 5 are X-ray diffraction patterns from carbon pyrolyzed at temperatures ranging from 300 to 2400 °C, along with dashed lines indicating the locations of the (0 0 2) and (1 0 1) graphite reflections. The two broad peaks (20–26° and 41–46°) that are visible in the patterns are characteristic of amorphous carbon,

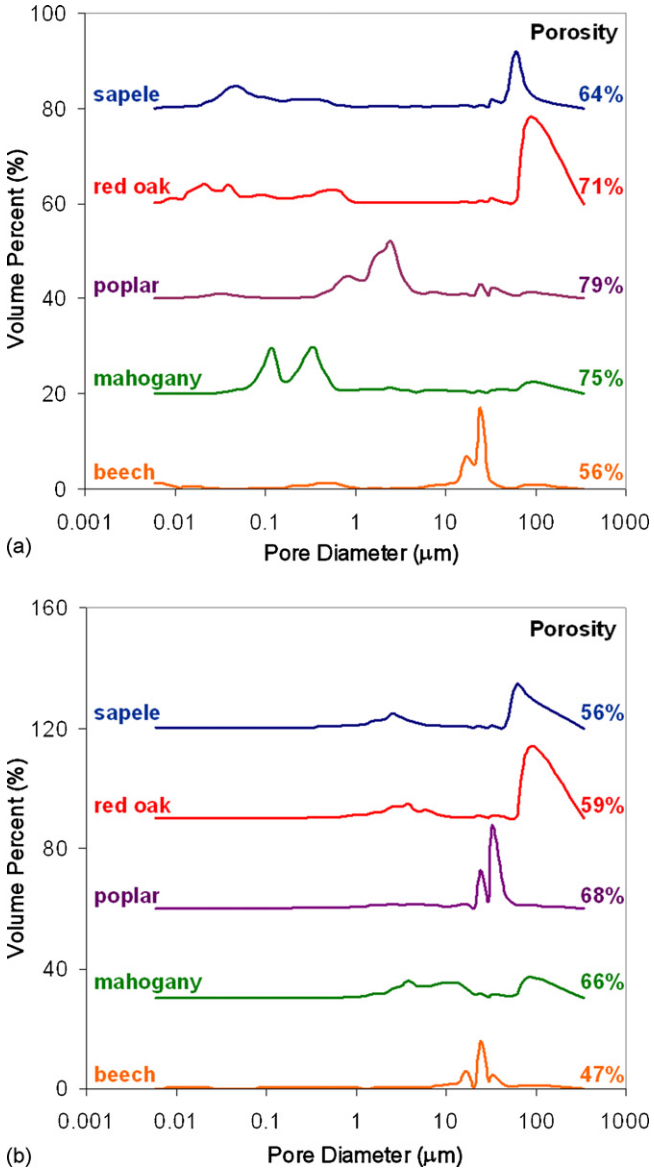

Fig. 3. Pore size distributions and porosities of (a) carbon samples pyrolyzed to 1000 °C and (b) silicon carbide samples derived from carbon pyrolyzed to 1000 °C from five wood precursors as determined by mercury porosimetry. Curves are offset by (a) 20 volume% and (b) 30 volume% for ease of viewing.

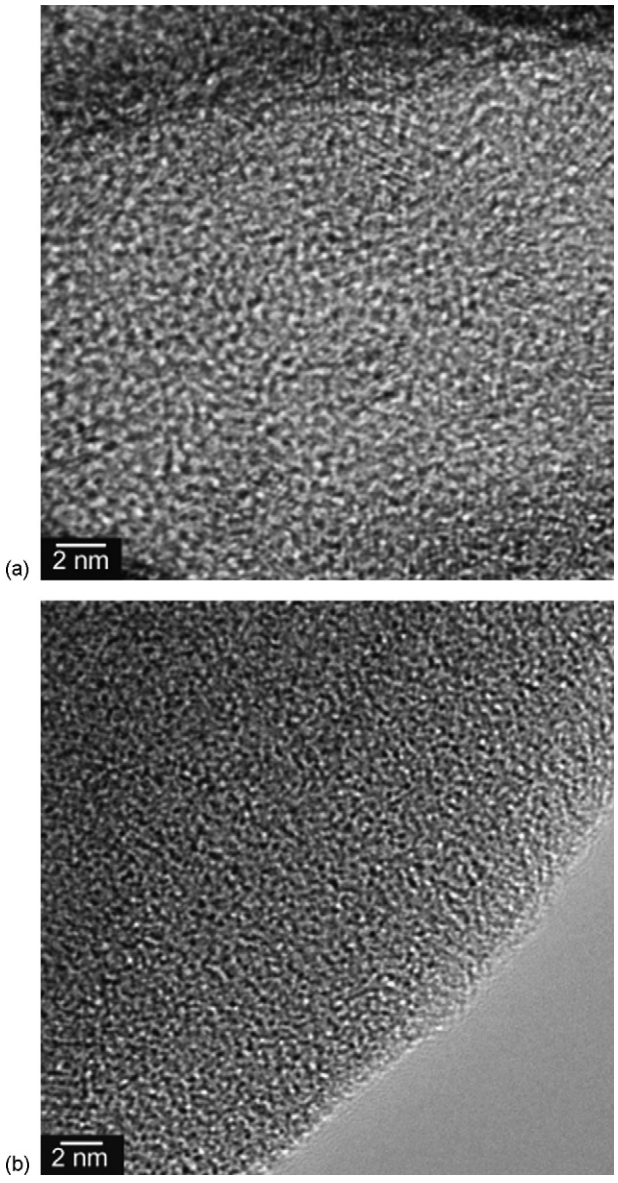

Fig. 4. High resolution transmission electron micrographs of (a) carbon 300 and (b) residual carbon present in bioSiC 1000.

and are present in the general vicinity of the (0 0 2) and (1 0 1) graphite reflections. The intensity and definition of the broad peaks are enhanced with higher pyrolyzation temperature. This is apparent when focusing on the amorphous ridge present near 44°, which is nearly flat in carbon pyrolyzed at 300 and 500 °C, compared to that in samples pyrolyzed at 1200 and 1500 °C, where much more definition is evident. The amorphous ridge in the vicinity of the (0 0 2) graphite reflection is shifted to the left several degrees from either the graphitic carbon or the turbostratic carbon reflections at 26.5° and 26°, respectively, signifying a larger characteristic *d*-spacing.[15] Only with carbon pyrolyzed at 2400 °C is there a well-defined peak, which occurs at 26°, indicative of turbostratic carbon. These results agree well with previous results for powdered poplar-based carbon, where resemblance to a well-defined peak was first seen at a pyrolysis temperature of 2500 °C.[10] The increase in definition of the broad carbon peaks with increasing pyrolysis temperature from 300–1500 °C and the ultimate formation of a turbostratic carbon peak at 2400 °C illustrate a slight increase in the degree of ordering and a trend towards a layered structure.

Further substantiation of ordering in the system with increased carbon pyrolyzation temperature is provided by Raman spectroscopy. The Raman spectra are shown in Fig. 6 for beech-based carbon samples pyrolyzed at temperatures from 300 to 2400 °C. The spectra reflect the subtle changes in the structure of the carbon that are not easily quantified in the X-ray diffraction patterns. D peaks represent the disorder in the system (D1: graphene layer edge disorder at 1350 cm^{-1}, D2: graphene layer surface disorder at 1620 cm^{-1}, and D3: amorphous carbon at 1500 cm^{-1}), while the G peak, at 1580 cm^{-1}, represents ordered graphitic structure.[16]

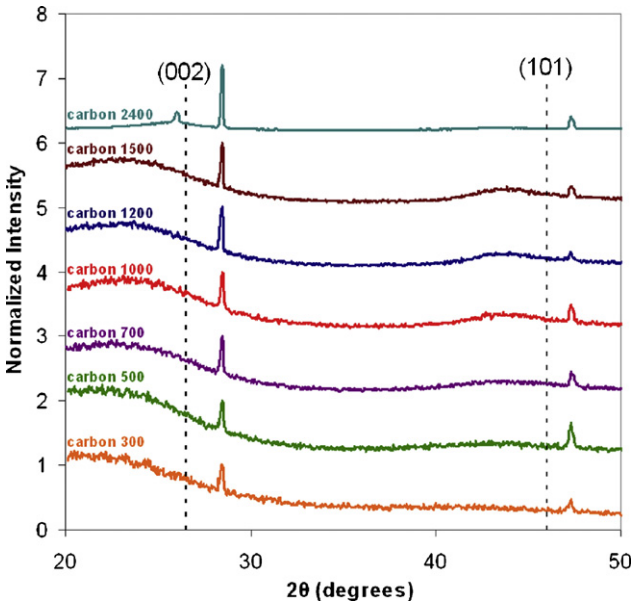

Fig. 5. X-ray diffraction of carbon pyrolyzed at different temperatures. The two sharp peaks in these patterns are due to the silicon standard. Curves are offset for ease of viewing.

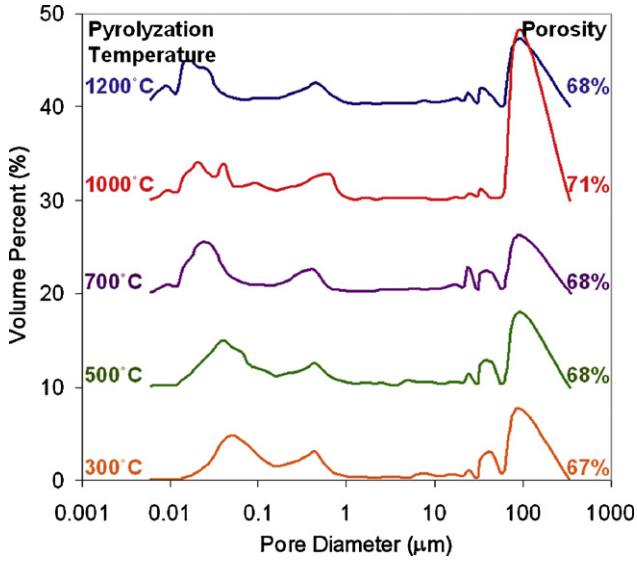

Fig. 7. Pore size distribution and porosities of carbon derived from red oak wood pyrolyzed at different temperatures as determined by mercury porosimetry. Curves are offset by 10 volume% for ease of viewing.

The spectra of samples pyrolyzed at lower temperatures have very broad D1 peaks which become more defined, evidenced by decreasing full width half maximum (FWHM) as the pyrolysis temperature increases, an indication of increased order. The D2 and G peaks overlap, resulting in a convoluted peak. The D3 peak manifests itself as the signal observed in the saddle region between the D1 and G peaks. At low pyrolysis temperatures, the D2 and G peaks are indistinguishable. As the pyrolyzation temperature increases, the D2 and D3 contributions decrease. This causes enhanced definition of the G peak with a shift towards its characteristic wavenumber, due to the appearance of a distinct, yet lower intensity D2 shoulder. Ultimately, at a pyrolyzation temperature of 2400 °C, there is a G peak at the expected position, with a higher intensity, indicating that the majority of the surface disorder (D2) and amorphous carbon (D3), respectively, are no longer present. However, the defined D1 peak shows that edge disorders (D1) remain, indicating that the resulting structure is turbostratic carbon, not graphite. This correlates well with the X-ray diffraction results shown in the previous section. Though graphite is never formed, it is apparent that there is progression towards increased order, as exemplified by the improved definition in both the D1 and G peaks, and the gradual decrease in intensity of the D2 and D3 peaks.

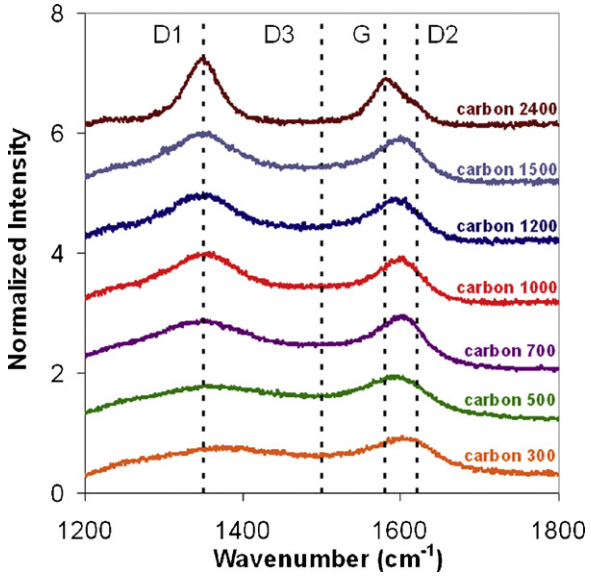

Fig. 6. Raman spectra of beech-based carbon pyrolyzed at temperatures from 300–2400 °C. Curves are offset for ease of viewing.

In addition to the bonding changes that the X-ray diffraction and Raman spectroscopy detect, microstructural changes in the carbon can be quantified on a microscopic level by using mercury porosimetry. Mercury porosimetry data, including porosity and pore size distributions, from red oak wood pyrolyzed at temperatures ranging from 300–1200 °C are presented in Fig. 7. As the carbon is pyrolyzed to higher temperatures, the pore size shifts to slightly smaller values, but the porosity volume fraction remains fairly constant. These changes are, in part, due to the decomposition of the organic matter and accompanying shrinkage of ~60%.[6]

While it is difficult to detect changes using microscopy alone, the combination of X-ray diffraction, Raman spectroscopy, and mercury porosimetry have proven to be more useful in detecting subtle differences between carbon pyrolyzed at different temperatures. As a result, it is clear that the carbon undergoes changes in the bonding, and at a microstructural level, changes in pore size, as a result of increased pyrolyzation temperature. The next step is to determine how this initial pyrolyzation temperature affects the resulting biomorphic silicon carbide.

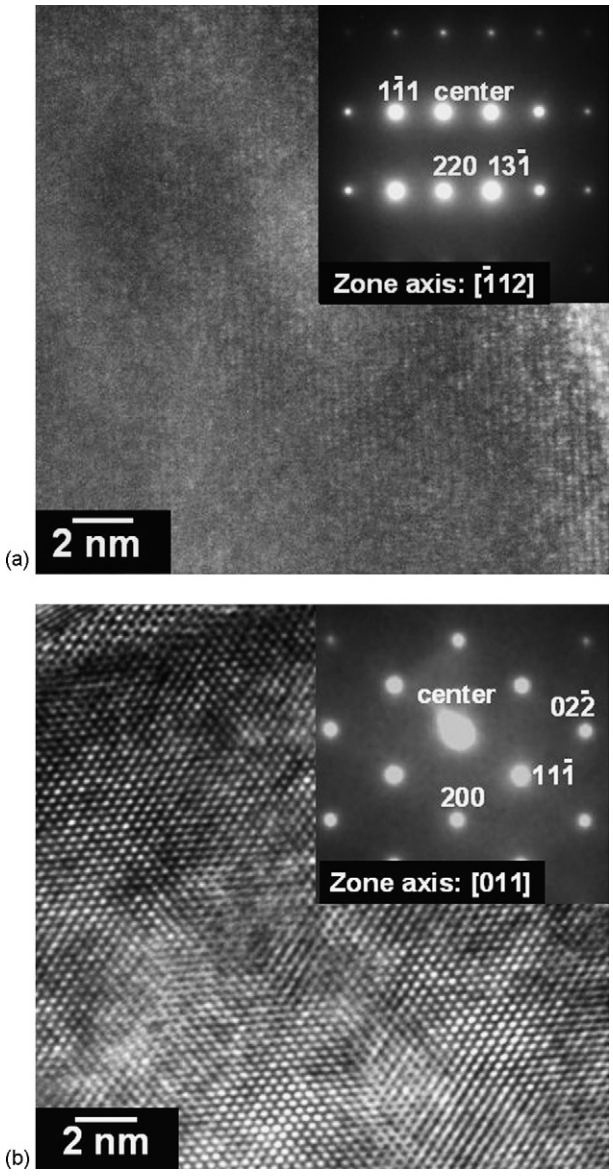

Fig. 8. High resolution transmission electron micrographs of the silicon carbide from (a) a bioSiC 300 sample and (b) a bioSiC 1000 sample.

3.3. Conversion to silicon carbide

Fig. 8 shows HRTEM images of bioSiC 300 and 1000. The two insets are the corresponding selected area electron diffraction (SAED) patterns, indicating that both bioSiC 300 and 1000 are cubic with lattice parameters of 4.355 ± .02 and 4.352 ± .02 Å, respectively. The lattice parameters calculated from SAED patterns agree well with the theoretical value of 4.3589 Å.[17] The HRTEM image of bioSiC 300 (Fig. 8(a)) along the [$\bar{1}$ 1 2] zone axis reveals that SiC is well crystallized. The HRTEM image of bioSiC 1000 along the [0 1 1] zone axis (Fig. 8(b)) also shows that SiC is fully crystallized with a long-range ordering. Both SAED patterns and HRTEM images indicate that the crystal structure of bioSiC is independent of initial carbon pyrolyzation temperature.

Fig. 9 shows the Raman spectra for silicon carbide processed from carbon pyrolyzed at 300–1200 °C. In the spectra, two features are present, due to transverse optical (TO, 796 cm^{-1}) and longitudinal optical (LO, 968 cm^{-1}) vibrations.[18] This figure clearly shows the prominent TO peak, which does not show any variation in peak height or shape as a function of initial carbon pyrolysis temperature. The LO peak is also visible, but difficult to resolve due to background noise present at similar wavenumbers. The consistency in the spectra from each silicon carbide sample indicates that, contrary to the carbon, where there was an apparent progression towards a higher degree of order, there is no change in the silicon carbide. Thus, the bonding in the silicon carbide is independent of initial carbon pyrolyzation temperature.

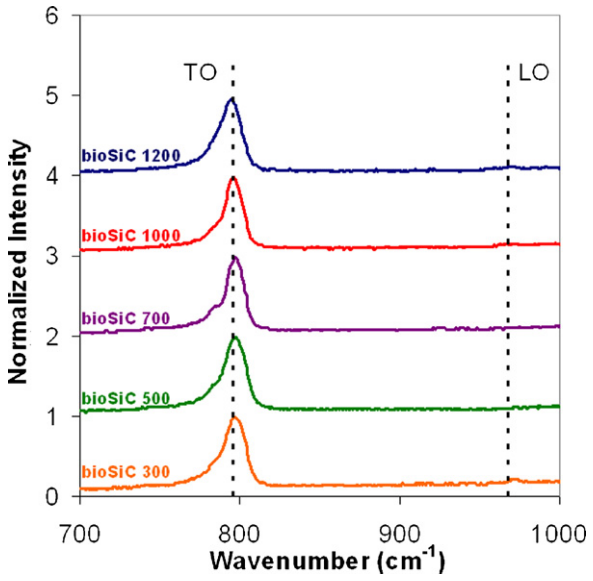

Fig. 9. Raman spectra of beech-based silicon carbide derived from carbon pyrolyzed to 300–1200 °C. Curves are offset for ease of viewing.

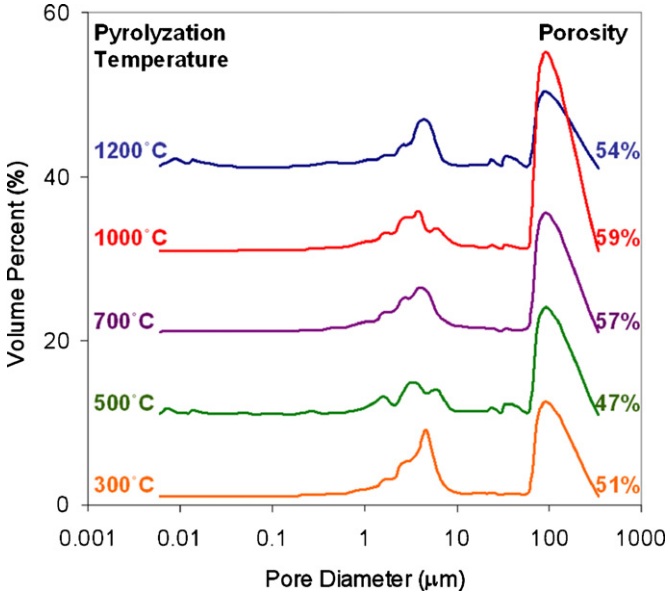

Fig. 10. Pore size distribution and porosities of silicon carbide derived from red oak wood pyrolyzed at different temperatures as determined by mercury porosimetry. Curves are offset by 10 volume% for ease of viewing.

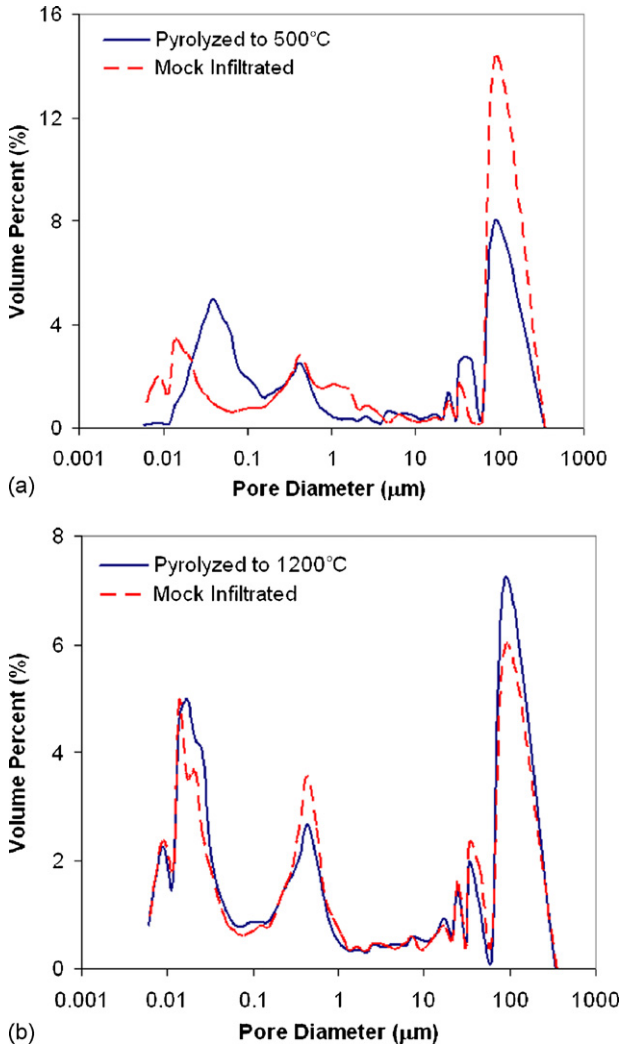

Fig. 11. Pore size distributions of red oak-based carbon (a) pyrolyzed at 500 °C followed by mock infiltration, and (b) pyrolyzed at 1200 °C followed by mock infiltration to 1500 °C.

Mercury porosimetry was used in order to gain a microscopic understanding of the bioSiC pore structure as a function of carbon pyrolyzation temperature. Fig. 10 shows the pore size distribution for red oak-based bioSiC derived from carbon pyrolyzed at temperatures ranging from 300–1200 °C. The porosities decreased by ~10% from pyrolyzed wood to silicon carbide, as the smaller pores, below 1 μm, close due to the ~58% volume expansion upon conversion to silicon carbide.[6] The distributions, however, do not vary significantly with initial carbon pyrolyzation temperature. One hypothesis for this is that during the infiltration step, prior to melting or vaporization of silicon, the carbon is heated in excess of 1200 °C, and pyrolyzation continues. This suggests that, regardless of the initial pyrolyzation temperature, the carbon specimens will be structurally comparable immediately prior to the start of infiltration. This ultimately leads to the similarities among the five pore size distributions in Fig. 10, indicating that the pore size distribution and porosity are independent of carbon pyrolyzation temperature for bioSiC materials.

3.4. Mock infiltration

To test the hypothesis that pyrolyzation continues during the infiltration step, carbon samples were subjected to a mock infiltration. Specifically, samples were heated to 1500 °C in a vacuum, under identical conditions to the infiltration step, but without the introduction of silicon. Fig. 11(a) and (b) show comparisons between red oak-based carbon initially pyrolyzed at (a) 500 °C and (b) 1200 °C, and their respective mock-infiltrated samples.

It is clear from Fig. 11(a) that microstructural changes occur between the initial pyrolyzation step at 500 °C and the subsequent mock infiltration. Akin to results shown in Fig. 7, where small pores shift to a smaller diameter with increasing pyrolyzation temperature, comparable alterations occur in the mock infiltration step. Fig. 11(b), indicates strong similarities in pore size distribution between the carbon pyrolyzed at 1200 °C and the mock-infiltrated sample. The results indicate that the carbon derived from the higher initial pyrolyzation temperature is similar to the carbon that is present immediately prior to infiltration. These experiments suggest that pyrolyzation continues to occur for an additional 1–3 h, depending on the initial pyrolyzation temperature, as the carbon is heated to the infiltration temperature before the silicon carbide formation reaction begins. This implies that in each infiltration reaction, the carbon is exposed to the same maximum temperature, and thus the same degree of pyrolyzation occurs before silicon infiltration, regardless of the initial pyrolyzation temperature. Hence, silicon carbide pore distributions are independent of the initial carbon pyrolyzation temperature.

4. Conclusions and implications

Carbon was pyrolyzed at temperatures ranging from 300–2400 °C, and silicon carbide was processed from carbon pyrolyzed at temperatures from 300–1200 °C. Transmission electron microscopy demonstrated that there is no visible difference in the structure of either carbon (amorphous) or silicon carbide (cubic crystalline) as a result of these processing schemes. X-ray diffraction indicated an increase in order in the carbon samples with an increased carbon pyrolyzation temperature, which was further confirmed by Raman spectroscopy. Raman spectroscopy was also performed on silicon carbide processed from carbon pyrolyzed at different pyrolyzation temperatures, and indicated no difference in the resulting vibrations. Thus, the microstructure of wood-derived silicon carbide is independent of carbon pyrolyzation temperature.

Although porosimetry showed evidence for a decrease in pore size as a function of higher pyrolysis temperature in the carbon and from conversion of carbon to silicon carbide, the silicon carbide pore distributions from carbon pyrolyzed at different temperatures illustrated no differences. Mock-infiltrated carbon illustrated that as the carbon is heated up during the infiltration step, the pyrolysis continues, and the resulting carbons have similar pore size distributions. These results explain the similarity in pore size distributions among bioSiC samples from different carbon pyrolysis temperatures. Hence, the initial

pyrolyzation temperature of wood prior to silicon infiltration can be as low as 500 °C yielding equivalent resulting silicon carbide materials, potentially lowering the energy required for bioSiC processing.

Acknowledgements

This work was funded by the National Science Foundation (DMR-0710630).

The SEM, TEM, and Raman Spectroscopy work was performed in the EPIC and Keck-II facilities of NUANCE Center at Northwestern University. NUANCE Center is supported by NSF-NSEC, NSF-MRSEC, Keck Foundation, the State of Illinois, and Northwestern University.

This work made use of the J.B. Cohen X-ray Diffraction Facility supported by the MRSEC program of the National Science Foundation (DMR-0520513) at the Materials Research Center of Northwestern University.

References

[1]. Ota, T., Takahashi, M., Hibi, T., Ozawa, M., Suzuki, S. and Hikichi, Y., Biomimetic process for producing SiC "Wood". *Journal of the American Ceramic Society*, 1995, **78**(12), 3409–3411.

[2]. Greil, P., Lifka, T. and Kaindl, A., Biomorphic cellular silicon carbide ceramics from wood: I. Processing and microstructure. *Journal of the European Ceramic Society*, 1998, **18**, 1961–1973.

[3]. Greil, P., Lifka, T. and Kaindl, A., Biomorphic cellular silicon carbide ceramics from wood: II. Mechanical properties. *Journal of the European Ceramic Society*, 1998, **18**, 1975–1983.

[4]. de Arellano-López, A. R., Martínez-Fernández, J., González, P., Domínguez, C., Fernández-Quero, V. and Singh, M., Biomorphic SiC: a new engineering ceramic material. *International Journal of Applied Ceramic Technology*, 2004, **1**(1), 56–67.

[5]. Wheeler, E., Wood: macroscopic anatomy. *Encyclopedia of Materials: Science and Technology, vol. 10*. Elsevier, New York, 2001.

[6]. Varela-Feria, F. M., Martínez-Fernández, J., de Arellano-López, A. R. and Singh, M., Low density biomorphic silicon carbide: microstructure and mechanical properties. *Journal of the European Ceramic Society*, 2002, **22**, 2719–2725.

[7]. Kaul, V. S., Faber, K. T., Sepúlveda, R. E., de Arellano López, A. R. and Martínez-Fernández, J., Precursor selection and its role in the mechanical properties of porous SiC derived from wood. *Materials Science and Engineering A*, 2006, **428**, 225–232.

[8]. Pappacena, K. E., Faber, K. T., Wang, H. and Porter, W. D., Thermal conductivity of porous silicon carbide derived from wood precursors. *Journal of the American Ceramic Society*, 2007, **90**(9), 2855–2862.

[9]. Byrne, C. E. and Nagle, D. C., Carbonization of wood for advanced materials applications. *Carbon*, 1997, **35**(2), 259–266.

[10]. Byrne, C. E. and Nagle, D. C., Carbonized wood monoliths—characterization. *Carbon*, 1997, **35**(2), 267–273.

[11]. Cheng, H-M., Endo, H., Okabe, T., Saito, K. and Zheng, G-B., Graphitization behavior of wood ceramics and bamboo ceramics as determined by X-ray diffraction. *Journal of Porous Materials*, 1999, **6**, 233–237.

[12]. Franklin, R. E., Crystallite growth in graphitizing and non-graphitizing carbon. *Proceedings of the royal society of London series A, mathematical and physical sciences*, 1951, **209**(1097), 196–218.

[13]. Miller, R. B., *Forest Products Laboratory Wood Engineering Handbook*. Prentice Hall, Englewood, 1990.

[14]. Washburn, E. W., The dynamics of capillary flow. *Physical Review*, 1921, **17**(3), 273–283.

[15]. Oya, A. and Marsh, H., Review: phenomena of catalytic graphitization. *Journal of Materials Science*, 1982, **17**, 309–322.

[16]. Sadezky, A., Muckenhuber, H., Grothe, H., Niessner, R. and Poschl, U., Raman microspectroscopy of soot and related carbonaceous materials: spectral analysis and structural information. *Carbon*, 2005, **43**, 1731–1742.

[17]. *JCPDS International Centre for Diffraction Data File 00–029-1129 (β - SiC)*, JCPDS International Centre for Diffraction Data, Newtown Square, PA; 2007.

[18]. Baek, Y., Ryu, Y. and Yong, K., Structural characterization of β-SiC nanowires synthesized by direct heating method. *Materials Science and Engineering C*, 2006, **26**, 805–808.